Tutor/s

Dr. Mohammed Salah El Fallah
*Departament de Química Inorgànica i Orgànica*

Grau de Química

# Treball Final de Grau

**Synthesis of new coordination complexes 3d and 4f with Schiff bases. Structural and magnetic studies.**

**Síntesi de nous complexes de coordinació 3d o 4f amb bases de Schiff. Estudi estructural i magnètic.**

Sergio Caballero Gutiérrez

*June 2021*

Universitat de Barcelona

B:KC Barcelona Knowledge Campus
Campus d'Excel·lència Internacional

*Un hombre con una idea nueva es un loco hasta que la idea triunfa.*

Mark Twain

Gràcies al Dr. Mohammed Salah per guiar-me durant aquests mesos de treball. Gràcies a tots els meus companys del laboratori de magnetisme molecular per donar-me els seus consells i ajudar-me en tots els dubtes que m'anaven sorgint. Gràcies als meus pares i a la meva família pel suport que m'han donat durant tots aquests anys d'aprenentatge.

# REPORT

# CONTENTS

**1. SUMMARY** 3
**2. RESUM** 5
**3. INTRODUCTION** 7
3.1. Schiff bases and their properties 7
3.1.1. Other ligands used in molecular magnetism 8
3.2. Magnetism 8
3.2.1. Initial considerations 9
3.2.2. Molecular magnetism 9
3.2.3. Lanthanide properties 11
3.2.4. Single Molecule Magnets 11
3.3. Crystallization techniques 12
3.4. Characterization techniques 13
**4. OBJECTIVES** 14
**5. RESULTS AND DISCUSSION** 15
5.1. IR spectra 15
5.2. Crystal structures 16
5.2.1. Crystal structure of compound 1 $[Cu_2(L1)_2ClO_4][Cu(L1')Cl](ClO_4)$ 16
5.2.1.2. Discussion 19
5.2.2. Crystal structure of compound 2 $[Mn_2(L2)_2(\mu^2\text{-}Cl_2)Cl_2]$ 19
**6. MAGNETISM STUDIES** 22
6.1. Magnetic properties of compound 1 22
6.2. Magnetic properties of compound 2 24
**7. EXPERIMENTAL SECTION** 27
7.1. Materials and methods 27
7.2. Synthesis of the $H_2L$ ligand 27
7.3. Synthesis of the complexes 27

7.3.1. Synthesis of compound 1 27
7.3.2. Synthesis of compound 2 28
**8. CONCLUSIONS** 29
**9. REFERENCES AND NOTES** 30
**10. ACRONYMS** 31
**APPENDICES** 33
Appendix 1: Other structures 35
Appendix 2: Crystallographic data 37

# 1. SUMMARY

The main goal of this work was to obtain 3d and 4f polynuclear coordination compounds with Schiff bases as ligands and the study of their magnetic and structural properties. A few trials were carried out using Ni(II), Mn(II), Cu(II), Gd(III) and Dy(III), although only two compounds using Cu(II) and Mn(II) were able to crystallize. Their structures were successfully determined by X-ray diffraction. The copper compound crystallized as a dinuclear unit with formula $C_{30}H_{30}Cl_2Cu_2N_6O_{14}$, and a monomeric unit with formula $C_{15}H_{17}Cl_2CuN_3O_3$ that co-crystallizes in the same crystal structure. The manganese complex was a dinuclear complex with formula $C_{30}H_{34}Cl_2Mn_2N_6O_4$ bridged by two chloride anions. Instead of the desired Schiff base, two new types of ligands were obtained due to an unexpected cyclization of one of the hydroxy groups leading to an oxazolidine ring in the first compound, and a rare double oxazolidine ring ligand that is able to complex the manganese (II) atoms in the second compound. Magnetic susceptibility measures were performed for both compounds. Compound 1 exhibits a weak antiferromagnetic coupling between the two Cu(II) metal ions, with an exchange constant J=-0.67 $cm^{-1}$. Compound 2 exhibits a very weak antiferromagnetic coupling between the two Mn(II) metal ions, with an exchange constant J=-0.24 $cm^{-1}$.

**Keywords**: Coordination chemistry, molecular magnetism, Schiff bases, oxazolidines

# 2. RESUM

L'objectiu principal d'aquest treball de fi de grau va ser l'obtenció de complexos de coordinació utilitzant metalls 3d i 4f amb bases de Schiff com a lligands i l'estudi de les seves propietats estructurals i magnètiques. Es van dur a terme diverses síntesis utilitzant Ni(II), Mn(II), Cu(II), Gd(III) i Dy(III), tot i que només dos compostos de Cu(II) i Mn(II) van cristal·litzar. El compost de coure cristal·litza com a una unitat dinuclear de fórmula $C_{30}H_{30}Cl_2Cu_2N_6O_{14}$, i una unitat monomèrica de fórmula $C_{15}H_{17}Cl_2CuN_3O_3$ que co-cristal·litza en la mateixa estructura cristal·lina. El segon compost es tracta d'un complex dinuclear de manganès de fórmula $C_{30}H_{34}Cl_2Mn_2N_6O_4$ unit per un pont format per dos clorurs. En lloc d'obtenir la base de Schiff desitjada, dos tipus de lligands es van formar degut a la inesperada ciclació d'un dels grups hidroxil del lligand, formant una oxazolidina en el primer compost i una doble oxazolidina en el segon compost que actua com a lligand dels àtoms de Mn(II). Es van dur a terme mesures de susceptibilitat magnètica en els dos compostos. El primer mostra un acoblament antiferromagnètic feble entre els dos ions de Cu(II), amb una constant d'intercanvi J=- 0,67 $cm^{-1}$. El segon compost presenta un acoblament antiferromagnètic molt feble entre els dos àtoms de Mn(II), amb una constant d'intercanvi J=-0,24 $cm^{-1}$.

**Paraules clau**: Química de coordinació, magnetisme molecular, bases de Schiff, oxazolidines

# 3. INTRODUCTION

## 3.1. SCHIFF BASES AND THEIR PROPERTIES

Schiff bases are an important type of organic ligand in coordination chemistry due to their ability to coordinate with most metallic cations to form complexes with interesting magnetic and structural properties. A Schiff base is a functional group that contains a carbon-nitrogen double bond, with the nitrogen atom bonded to an aryl or alkyl group. They are easily synthesized by the condensation of a primary amine with an aldehyde or ketone. The mechanism of the reaction proceeds as follows: the lone pair of the nitrogen attacks the carbonyl giving a hemiaminal, which quickly undergoes a hydrogen shift, thus favouring the loss of a water molecule. In this work, pyridine-2-carboxaldehyde and 2-amino-1,3-propandiol were used to synthetize the Schiff base ligand $H_2L$ ((*E*)-2-((pyridin-2-ylmethylene)amino)propane-1,3-diol).

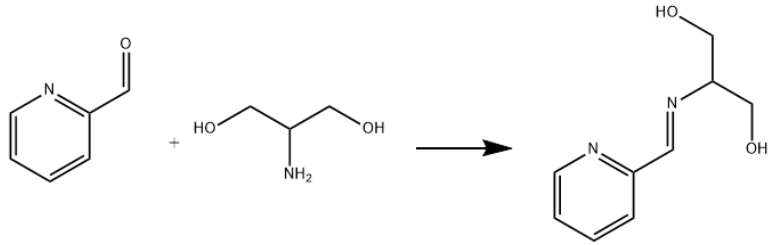


Fig. 1. Synthesis of the Schiff base used in this work ($H_2L$)

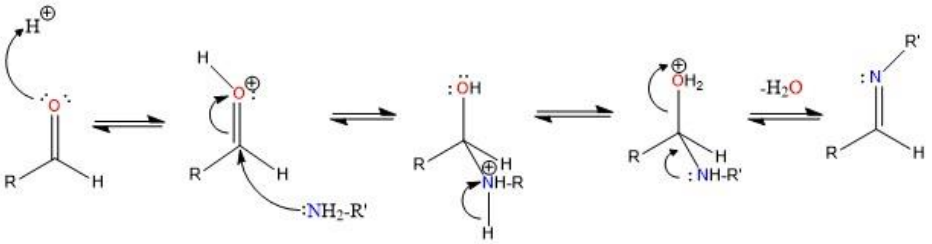


Fig. 2. Imine formation mechanism

Owing to the fact that ligands containing Schiff bases may have different types of donor atoms, they can coordinate both transition metals and lanthanides in the same structure, giving rise to new compounds with interesting magnetic properties.

As we will see on the next section, a different reaction might take place depending on the conditions of the experiment and the position of the hydroxo groups that are present on the aminoalcohol used in this work. One of the oxygen atoms from the hydroxo groups may attack the carbon from the C and form an oxazolidine (a five-membered ring containing an oxygen and a nitrogen atom on the 1 and 3 positions respectively). Despite being an unexpected reaction, oxazolidines are well known for their interesting properties (p. e. chiral auxiliary for asymmetric synthesis). They can be used as a ligand for the development of asymmetric catalysts, among other applications. [1]

### 3.1.2. Other ligands used in molecular magnetism.

A wide variety of co-ligands can be used to give different structural and magnetic properties (p. e. halides, pseudohalides, dicyanamide, carboxylates, oxalates and nitrites, among others). For example, azido bridges are widely used because of their versatility: they display various coordination modes in polynuclear transition complexes, the most common of them being end-on (1,1), double end-on and end-to-end (1,3). Depending on these modes, a different magnetic interaction can be transmitted between the metallic centres.

β-diketonates are another important group of co-ligands used in molecular magnetism because they can efficiently coordinate both transition metals and lanthanides due to the strong coordinating character of the deprotonated β-diketonate group. This anion has a great coordinating ability since negatively charged O atoms can coordinate more than one metal ions.

Some of these co-ligands have been used during this work, although no compounds could be obtained.

## 3.2. MAGNETISM

In coordination chemistry, the magnetic properties of complexes arise when a paramagnetic metal is present, which means that they have unpaired electrons. These electrons possess magnetic moments as a result of their orbital and spin angular moments, and both these moments interact with an external magnetic field.

### 3.2.1. Initial considerations

When a polyelectronic metal with unpaired electrons interacts with a coordination environment, different perturbations modify the energies of the electrons, giving rise to the energy

terms. In transition metals, the most significant perturbations are due to the interelectronic repulsions and the electrostatic potential around the cation (crystal field) generated by the surrounding ligands. These energy terms may be affected by lower energy perturbations, such as spin orbit coupling and the Zeeman effect, which is derived from the application of an external magnetic field. These perturbations induce the splitting of the terms in level and sublevels, splitting the terms or multiplets from the crystal field to give magnetic states ($m_j$) [2].

### 3.2.2. Molecular magnetism

When a complex with unpaired electrons is placed within an external magnetic field H, it becomes magnetized, which means that the electrons in the sample become aligned with the field. This phenomenon is known as magnetization, and it can be expressed in terms of magnetic susceptibility ($\chi$). Every complex has a diamagnetic susceptibility due to the paired electrons of the inner orbitals. The total susceptibility measured in a sample is the sum of the diamagnetic and paramagnetic contributions. The diamagnetic contribution can be calculated using Pascal tables or using equation 1. Usually, in molecular magnetism, susceptibility measures are calculated as $\chi_M T$, where $\chi_M$ is the molar susceptibility.

$$\chi = \chi_{param.} - \chi_{diam.} \qquad \text{(Eq. 1)}$$

Let us consider a simple dinuclear complex with two paramagnetic cations bridged by a diamagnetic ligand. From a magnetic point of view, these cations can either act independently, giving a paramagnetic compound, or they can interact between them giving a new molecular paramagnetic compound. This behaviour is due to the fact that the linear combination of the d-orbitals of the metals and the p orbital of the ligand gives rise to three molecular orbitals: one fully occupied bonding orbital, one non-bonding orbital and an antibonding orbital, with the highest energy. Two electrons are placed in the bonding orbital and do not have a magnetic contribution. The other two electrons may go either both into the non-bonding orbital ($S_T$=0 spin singlet) or one in the non-bonding and the other in the antibonding orbital. ($S_T$=1, spin triplet). If the ground state is a spin singlet, we say that the interaction is antiferromagnetic, and if the ground state is a spin triplet, the interaction is ferromagnetic [2].

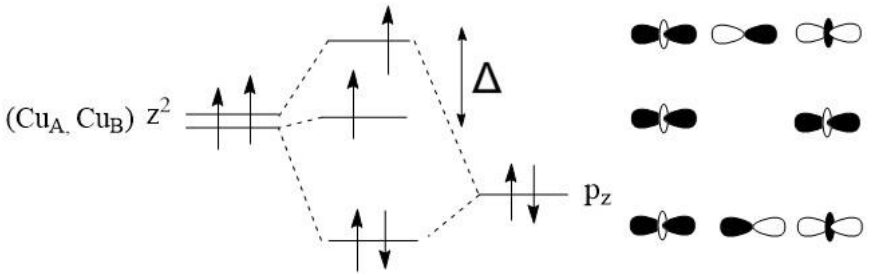


Fig. 3. Bonding scheme of a simple dinuclear copper (II) system when the ground state is a spin triplet ($S_T$=1).

The Heisenberg-Dirac-Van Vleck Hamiltonian (HDVV) describes the interaction between the spins of these two metallic centres, also known as exchange:

$$\hat{H} = -J_{AB}\hat{S}_A\hat{S}_B \qquad \text{(Eq. 2)}$$

where $J_{AB}$ is the exchange constant between both spins ($S_A$ and $S_B$) and it is measured in $cm^{-1}$. J<0 corresponds to an antiferromagnetic coupling, whereas J>0 corresponds to ferromagnetic coupling. If J<0, $\chi_M T$ tends to 0 $cm^3 K mol^{-1}$ at 0 K because S in the ground state is 0 while if J>0, $\chi_M T$ tends to 1 $cm^3 K mol^{-1}$, because S in the ground state is 1, as expected for two coupled electrons (in the case of a dinuclear copper (II) complex, see fig. 4). The magnitude of J is the sum of the contribution of the ferro (F) and antiferromagnetic (AF) components. $J_F$ depends on the exchange integral between the two magnetic orbitals, which means that a large overlap between orbitals results in a larger $J_F$. $J_{AF}$ is proportional to the square of the energy gap between the symmetric and antisymmetric molecular orbitals ($\Delta^2$, see fig. 3)

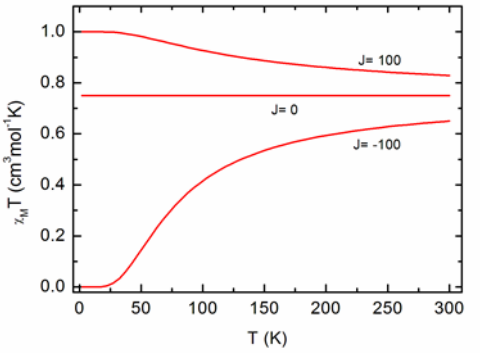


Fig. 4. Representation of a plot of $\chi_M T$ versus T.

### 3.2.3. Lanthanide properties

The magnetic properties of the lanthanide metals are quite different from those of the transition metals. In a lanthanide atom, the 4f orbitals are highly contracted and shielded by the fully occupied 5s and 5p orbitals, so the crystal field effect is much smaller than both the interelectronic repulsion and the spin-orbit coupling [3]. Because of this, the orbital momentum of the electrons is not negligible, which results in a large spin-orbit coupling. The trivalent rare earth metals 2S+1L multiplets are further split by spin-orbit coupling to give J states. The ligand-field effect in lanthanides is weaker than interelectronic repulsions and spin-orbit coupling. In fact, the crystal field splitting of f-orbitals is a about 1% that of d-orbitals. The energy spectrum of these states can be calculated as:

$$E\left(\left(^{2S+1}L_J\right) = \left(\frac{\lambda}{2}\right)[J(J+1) - L(L+1) - S(S+1)] \qquad \text{(Eq. 3)}$$

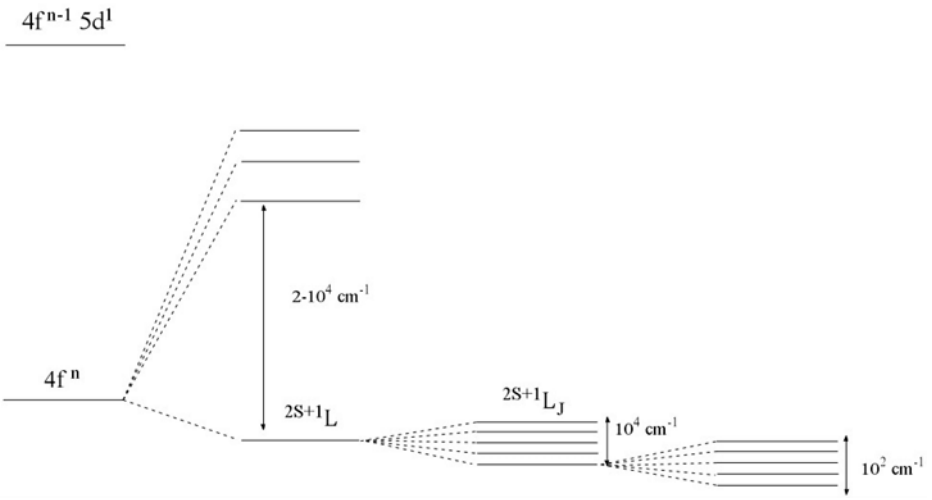


Fig 5. Splitting of the energy terms of a Ln(III) ion under different perturbations (Interelectronic repulsion, spin-orbit coupling, crystal field, magnetic field).

### 3.2.4. Single molecule magnets

Single molecule magnets (SMM) are a series of molecular based systems that, under a certain temperature value Tc, show slow relaxation of the magnetization, i.e., they behave as tiny

magnets. *Gatteschi* et al. discovered this phenomenon at the beginning of the 1990s [4]. These types of systems consist of discrete molecules or molecular clusters with a large total spin S in the ground state and a strong magnetic anisotropy. In these systems, the application of a magnetic field leads to the splitting of the $S_T$ levels into $m_s$ sublevels. The anisotropy of these systems is described by the Hamiltonian $\hat{H}=DS_z^2$, where D is the zero-field splitting parameter. When an external magnetic field is applied, the magnetic moment of the molecule lines up in one of the two possible directions. Both states are separated by an energy barrier $U_{eff}$, the maximum value of which is $-DS^2$ for an integer spin and $-D(S^2-1/2)$ for a half integer spin. The states with a negative $M_s$ are stabilized because they are parallel to the applied field. On the other hand, the states with a positive $M_s$ are destabilized because they correspond to magnetization against the applied field. The energy potential between these two states takes the shape of a double well (see figure 4), with the potential barrier ($U_{eff}$) in between. The magnetization is relaxed through different relaxation mechanisms, one of them being quantum tunnelling. The key factor for obtaining SMM is having a large magnetic anisotropy and a large magnetic moment. Because of this, lanthanides are the best candidates. Continuous efforts on synthetizing SMM's are being made due to their potential applications, such as high density data storage, quantum computing and spintronics [5].

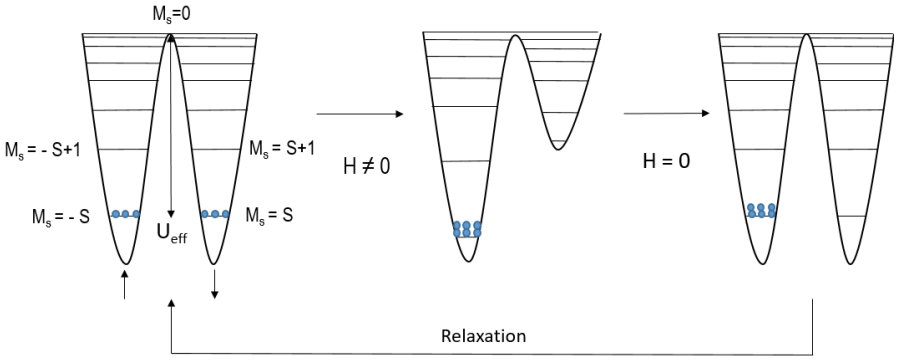


Fig. 6. Double well diagram representing the potential energy when a magnetic field is applied.

## 3.3. CRYSTALLIZATION TECHNIQUES

In order to know the structure of the obtained compound, monocrystal X-ray diffraction (XRD) is used. However, the difficulty of this technique lays on the fact that the obtention of a single crystal is usually hard. Therefore, we need various techniques that allow us to obtain good-sized crystals with a decent quality, suitable for XRD structural determination.

Slow evaporation: a vial with the complex solution is left undisturbed in open atmosphere until it reaches the saturation point and crystals start to appear.

Layer crystallization: it allows crystals to grow based on the difference of the complexes solubility in the solvent and the antisolvent (precipitating agent). The antisolvent is placed on the bottom of a glass tube and then, the complex solution is injected carefully using a glass syringe at the bottom of the glass tube. The antisolvent must have a lower density than the solution. Usually, diethyl ether is used.

Vapour diffusion: the principle is the same as in the layer crystallization technique, but in this case, the solution and the antisolvent are placed separately in a closed vial. As the antisolvent slowly diffuses into the solution, the solubility of the complex decreases until it precipitates as crystals.

## 3.4. CHARACTERIZATION TECHNIQUES

As previously mentioned, in molecular magnetism we need a way to elucidate the structures of the compounds that we manage to obtain in the laboratory.

XRD: This technique uses the diffraction of a beam of X-ray to determine the exact structure of the compounds. The way this beam is diffracted depends on the crystal structure of the complex. The data obtained in this technique provides information of the molecular structure in the space.

IR spectra: This technique gives information about the different functional groups that the compound may have depending on the wavelength at which these compounds absorb IR light. It does not provide any information about the disposition of the atoms.

# 4. OBJECTIVES

The main objectives of this work are:

- Synthesis and characterization of the Schiff base ligand ((*E*)-2-((pyridin-2-ylmethylene)amino)propane-1,3-diol.
- Design and synthesis of new polynuclear 3d ($Mn^{2+}$, $Ni^{2+}$, $Cu^{2+}$) and 4f ($Gd^{3+}$, $Dy^{3+}$) coordination complexes using the previously synthesised Schiff bases as ligands and other anions as co-ligands.
- Obtention of a single crystal (monocrystals) of the complexes suitable for XRD using various crystallization techniques.
- Structural determination of the complexes using XRD.
- Study of the magnetic properties of the complexes.
- Establish possible magneto-structural correlations of the complexes.

# 5. RESULTS AND DISCUSSION

## 5.1. IR SPECTRA OF THE COMPLEXES

The infrared spectra (4000-400 cm-1) of both compounds were collected on a Nicolet 5700 FT-IR spectrophotometer. Both spectra are presented in fig. 7 above and the peak assignment of the most significant bands is shown in table 1 and table 2 below.

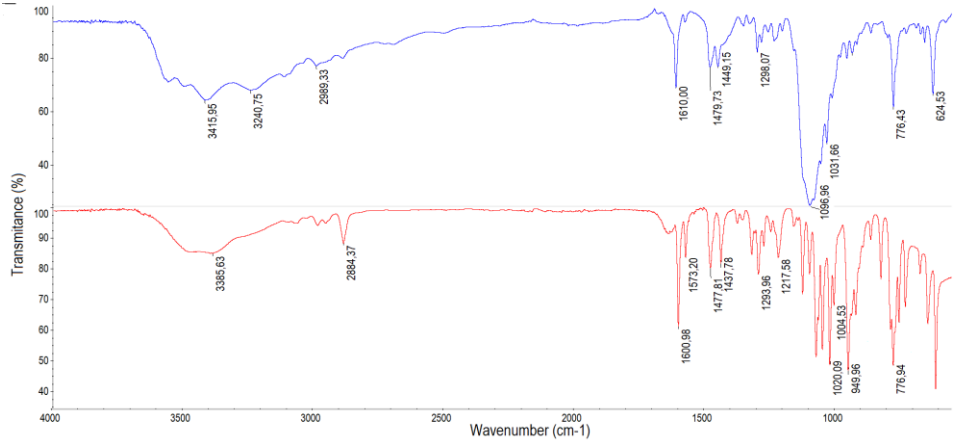


Fig. 7. IR spectra of compound 1 (top) and compound 2 (bottom).

| Peak (cm-1) | Assignment |
|---|---|
| 3415 | N-H stretching |
| 3240 | O-H stretching |
| 1610 | C=N stretching |
| 1479 | C-H δ |
| 1096 | $ClO_4^-$ |
| 1013 | C-O stretching |

Table 1. IR bands and assignment of compound 1.

| Peak | Assignment |
|---|---|
| 3475 | O-H stretching |
| 2884 | C=C aromatic |
| 1601 | C=N stretching |
| 1477 | C-H δ |
| 1020 | C-O asymmetric stretching |
| 945 | C-O symmetric stretching |

Table 2. IR bands and assignment of compound 2.

## 5.2. CRYSTAL STRUCTURES

### 5.2.1. CRYSTAL STRUCTURE OF COMPOUND 1 $[Cu_2(L_1)_2ClO_4][Cu(L_1')Cl](ClO_4)$

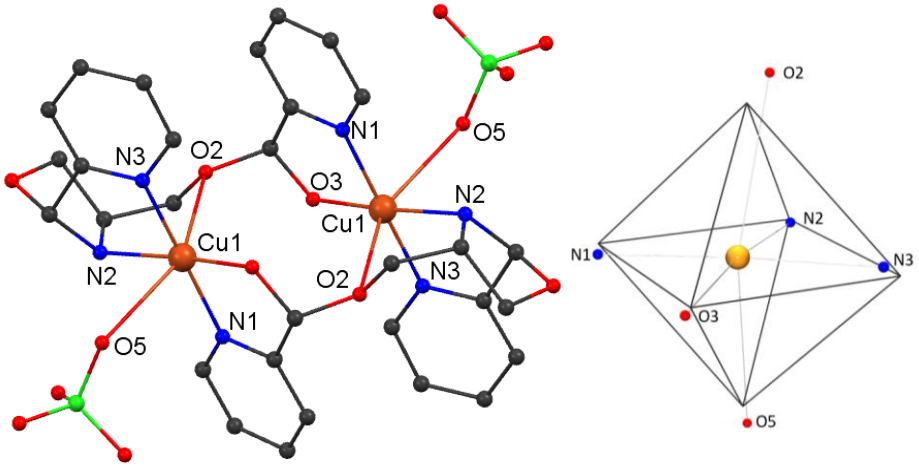


Fig. 8. (Left) Partially labelled structure of the dinuclear complex in compound 1 (hydrogen atoms omitted for clarity). (Right) Coordination polyhedron of the copper (II) atom in the dinuclear complex in compound 1 (the solid lines represent the ideal octahedron)

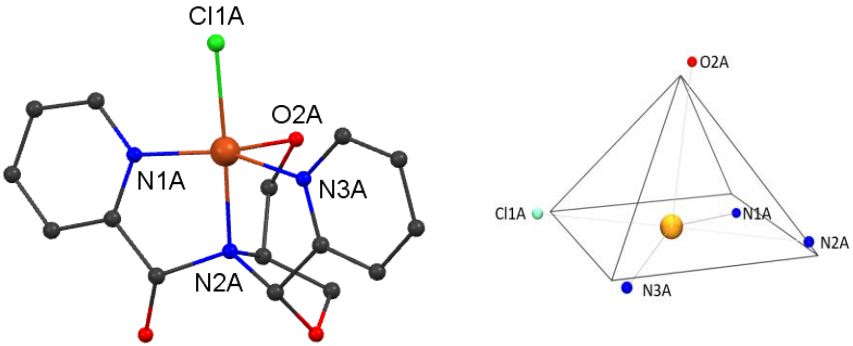


Fig. 9. (Left) Partially labelled structure of the mononuclear complex in compound 1 (hydrogen atoms omitted for clarity). (Right) Coordination polyhedron of the copper (II) atom in the mononuclear complex in compound 1 (the solid lines represent the ideal square-planar pyramid).

The single-crystal X-ray structure of compound 1 shows that it crystallizes in the triclinic space group P-1. The analysis reveals the formation of a neutral dinuclear copper complex and a positively charged mononuclear complex. In the dinuclear unit, each copper atom is hexacoordinated with a distorted octahedral $CuO_3N_3$ coordination sphere. Two units of a newly formed ligand and a perchlorate anion surround each copper atom in the dinuclear complex, where one ligand unit acts as a tridentate chelate for one copper atom and a bidentate chelate for the other copper atom. The Cu-O coordination distances vary in the range between 1.910 and 2.686 Å due to the presence of three different types of O-donors. The same applies for the Cu-N distances, which vary between 1.993 and 2.032 Å due to the presence of two different types of N-donors. The coordination geometry of the copper atom in the cationic monomer is square pyramidal with the basal coordination plane provided by one oxygen atom, four nitrogen atoms and a chloride anion at the tip of the pyramid. The Cu-O distance is 2.276 Å and the Cu-N distances vary from 1.976 to 2.055 Å. The intermetallic Cu-Cu distance is significantly large, 4.361 Å. The distortion of the coordination sphere of the Cu(II) ions in compound 2 has been calculated using the SHAPE v2 program based on continuous shape measures (CShM). CShM allows us to determine the distances between the ideal coordination environment and our real structure, yielding a deviation from the ideal polyhedron of 3.689. Valence bond calculations have been performed in the coordination sphere of the copper (II) atoms, giving a value of 2.21.

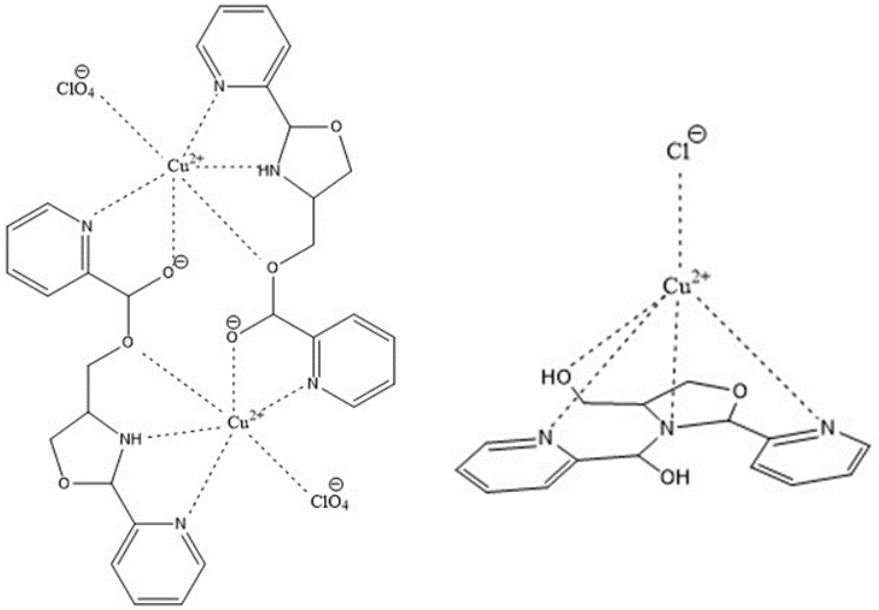


Fig.10. (Left) Schematic representation of the dinuclear complex in compound 1. (Right) Schematic representation of the neutral mononuclear complex in compound 1.

| Bond | Distance (Å) | Atoms | Angle (º) |
|---|---|---|---|
| Cu(1)- Cu(1) | 4.361 | N(1)-Cu-O(2) | 98.97 |
| Cu(1)-O(3) | 1.910 | N(1)-Cu-O(3) | 84.12 |
| Cu(1)-N(3) | 1.993 | N(1)-Cu-O(5) | 87.05 |
| Cu(1)-N(1) | 1.995 | N(1)-Cu-N(2) | 97.82 |
| Cu(1)-N(2) | 2.032 | N(1)-Cu-N(3) | 177.29 |
| Cu(1)-O(2) | 2.517 | O(2)-Cu-O(3) | 113.09 |
| Cu(1)-O(5) | 2.686 | O(2)-Cu-O(5) | 151.83 |
| Cu(2)-N(3a) | 1.976 | O(3)-Cu-O(5) | 94.83 |
| Cu(2)-N(1a) | 1.987 | | |
| Cu(2)-N(2a) | 2.055 | | |
| Cu(2)-Cl(1a) | 2.239 | | |
| Cu(2)-O(2a) | 2.277 | | |

Table 3. Bonding parameters of the dinuclear copper complex in compound 1.

### 5.1.2.2. DISCUSSION

It is clear that the structures obtained are not the desired Schiff base compounds that we were looking for. A new oxazolidine ring has been formed, and an additional pyridin-2-carboxaldehyde molecule has condensed with another ligand unit. This could be as a result of the reported compound being prepared by mixing the pyridine-2-carboxaldehyde, the amino-alcohol and the copper salt without refluxing. This was done to avoid heating perchlorate salts. The ring-closure reaction takes place because the cyclization of a five membered ring is usually favoured. Furthermore, it is believed that, in the presence of a complexed metallic cation, the imine bond may be polarized, increasing the electrophilic character of the iminic carbon, facilitating the nucleophilic attack of one of the two hidroxyl groups. On the mononuclear complex, the same cyclization has taken place, but in this case, the condensation between the ligand and the aldehyde proceeds through the nitrogen, creating a new nitrogen-carbon bond. It is unclear how and why these reactions have taken place.

## 5.2.2. CRYSTAL STRUCTURE OF COMPOUND 2 $[Mn_2(L2)_2(\mu^2\text{-}Cl_2)Cl_2]$

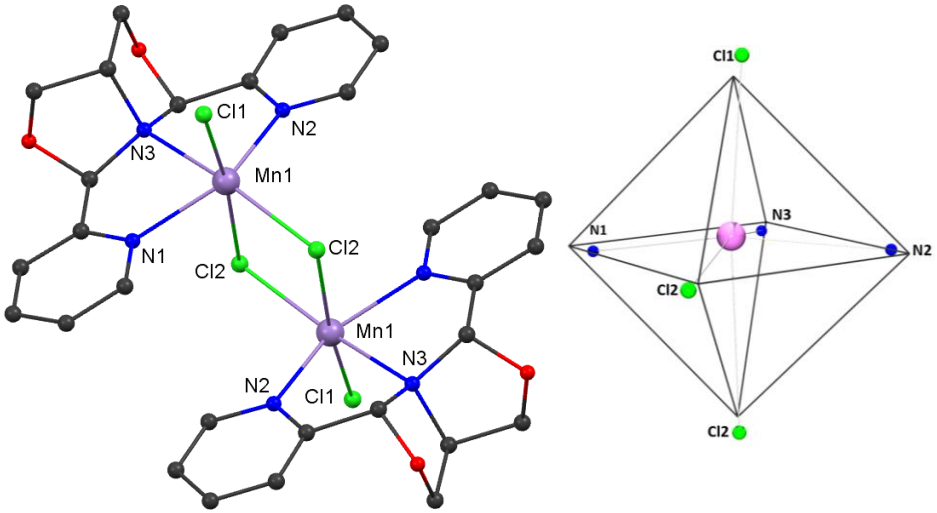


Fig. 11. (Left) Partially labelled structure of complex 2 (hydrogen atoms omitted for clarity). (Right) Coordination polyhedron of the manganese (II) atoms in complex 2 (the solid lines represent the ideal octahedron)

The single crystal X-ray structure of complex 2 shows that it crystallizes in the space group C2/c. The structure is shown in fig. 11. The analysis reveals the formation of a symmetrical dinuclear manganese (II) neutral complex bridged by two chloride anions ($\eta^2$). Each manganese atom is hexacoordinated with a significantly distorted octahedral $MnCl_3N_3$ coordination sphere. The formed ligand acts as a tridentate chelate that coordinates the metal through its three nitrogen atoms adopting the *mer* conformation around the cation. Additionally, each manganese atom is coordinated by a terminal chloride anion. The Mn-N distances vary between 2.205 Å and 2.367 Å due to different N donors. The Mn-N distances for the two pyridine nitrogen atoms are significantly shorter than the one for the tertiary amine nitrogen atom. This reflects the strong coordination ability of the pyridine nitrogen. The distance between the manganese atom and the axial Cl2 is 2.789 Å, while the distance with the equatorial Cl2 is 2.443 Å. The distance between the manganese atom and the terminal Cl1 is 2.455 Å. The main contributions to the distortion are the N-Mn-N and the Cl-Mn-Cl angles. The axial Cl1-Mn-Cl2 angle is 174º, which results in an almost linear arrangement. The Mn-Cl2-Mn angle is 94.54º and the Cl2-Mn-Cl2 angle is 85.47º. The intermetallic distance between both manganese atoms is 3.850 Å, significantly shorter than in the first structure. All these results are consistent with other complexes containing the $[Mn_2(\mu\text{-}Cl)_2]^{2+}$ unit found in the literature [6], [7], [8].

The ideal coordination polyhedron of complex 2 was measured using SHAPE v2 software. The central cation coordination geometry shows a deviation from the ideal octahedron of 2.449. Valence bond calculations have been performed in the coordination sphere of Mn(II), giving a deviation from the ideal polyhedron of 2.01. By looking at these results, it is expected that the ferro- or antiferromagnetic interactions between the manganese atoms through the chloride bridges will be very weak, if there is any interaction at all.

This time, a double cyclization process has taken place due to the electrophilic character of the iminic carbon, increased by the presence of a metal cation that acts as a catalyst, and the high stability of the newly formed five-membered rings. The cyclization leading to an oxazolidine ring is not rare and it has been reported before in the literature [1], [9], [10], although Saleem *et al*. reported that the reaction may take place even in the absence of a metal cation. However, the double cyclization step leading to a dinuclear complex has only been reported twice before: in a dinuclear iron complex [11] and in a mononuclear copper complex [12]. A proposed mechanism for the double cyclization is shown in fig. 12 below [13].

| Bond | Distance (Å) | Atoms | Angle (º) |
|---|---|---|---|
| Mn-N(1) | 2.206 | Cl(2)-Mn-Cl(2) | 85.47 |
| Mn-N(2) | 2.211 | Cl(2)-Mn-Cl(1) | 174.34 |
| Mn-N(3) | 2.370 | Mn-Cl-Mn | 94.53 |
| Mn-Cl(1) | 2.455 | N(2)-Mn-Cl(1) | 103.25 |
| Mn-Cl(2) (axial) | 2.789 | N(3)-Mn-Cl(1) | 97.64 |
| Mn-Cl(2) (equatorial) | 2.443 | N(1)-Mn-Cl(1) | 92.38 |
| | | N(2)-Mn-Cl(2) | 102.31 |
| | | N(3)-Mn-Cl(2) | 166.27 |
| | | N(1)-Mn-Cl(2) | 105.77 |
| | | N(1)-Mn-N(2) | 146.09 |
| | | N(1)-Mn-N(3) | 73.99 |

Table 4. Selected bond parameters of complex 2

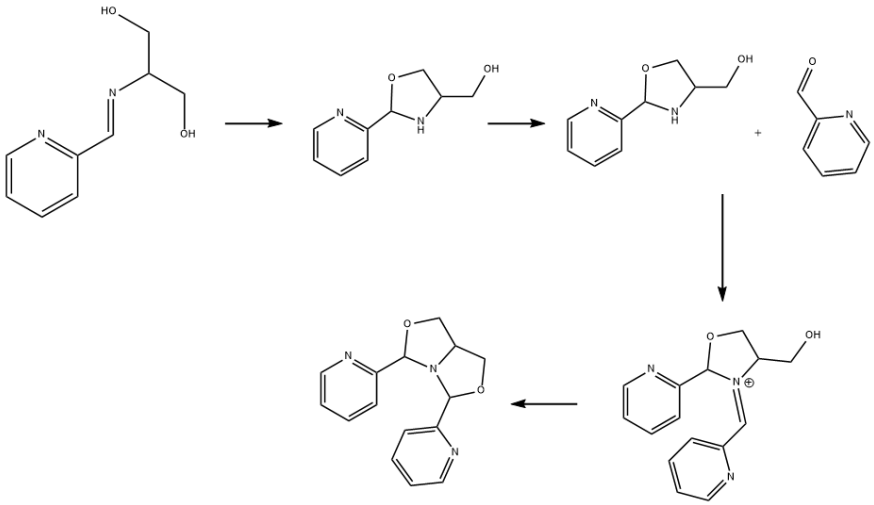

Fig. 12. Proposed reaction pathway of the double cyclization of the ligand in compound 2.

# 6. MAGNETISM STUDIES

Magnetic susceptibility measurements for the compound were carried out on polycrystalline samples, at the Servei de Magnetoquímica of the Universitat de Barcelona, with a Quantum Design SQUID MPMS-XL susceptometer apparatus working in the range 2-300 K under a magnetic field of approximately 5000 G (from 2-300 K) and 300 G (from 2-30 K). Diamagnetic corrections were estimated from Pascal Tables.

## 6.1. MAGNETIC PROPERTIES OF COMPOUND 1

The $\chi_M T$ value for compound 1 at 300 K is 0.790 $cm^3 mol^{-1} K$ for two copper (II) ions, which is as expected for two isolated copper (II) ion with g = 2.05. The $\chi_M T$ values are almost constant until ca. 40 K and then it decreases sharply, giving the minimum value of 0.667 $cm^3 K mol^{-1}$ at 2K as it shown in figure 13. The drop in $\chi_M T$ at low temperatures indicates the presence of a very weak antiferromagnetic coupling between the copper (II) ions.

As it is indicated in the description of the structure paragraph, the structure of compound 1 consist of two copper ions linked between the fragment formed by a carbon-oxygen-carbon bridge giving a dinuclear system. Thus, one coupling parameter J can be considered to interpret the magnetic interaction in the complex and the magnetic susceptibility can be fitted with the Bleaney-Bowers equation (equation 1) for a couple of S = 1/2 spins [14].

$$\chi T = \frac{2N_A g^2 \mu_B^2}{k} \cdot \frac{1}{3+e^{\frac{-J}{kT}}} \qquad \text{(Eq. 4)}$$

The parameters N, μB and K in the equation have their usual meanings. The best fit parameters from 300 down to 2 K are found as J = -0.67 $cm^{-1}$ and g = 2.05 with an error $R = 3.97 \cdot 10^{-5}$ for compound 1, where $R = \Sigma[(\chi_M T)_{exp} - (\chi_M T)_{calc}]^2 / \Sigma[(\chi_M T)_{exp}]^2$.

The magnetization measurements at 2 K up to an external field of 5.5 T confirm the very weak antiferromagnetic interaction. At a higher field, the reduced molar magnetization M/Nβ units tends to 1.88 (Figure 14). This value is slightly less to the expected for two isolated Cu(II) ion (2 M/Nb with g = 2.0), which is consistent with a very weak antiferromagnetic interaction. This confirms that if J is small, the XT product will be close to the expected value for two non-coupled electrons. This result is consistent with another dinuclear copper complex found in the literature [15].

This behaviour is expected because there is more than one diamagnetic atom acting as a bridge between the metallic centres, so there is not almost any exchange interaction between the copper atoms through the ligand. Due to the very long intermetallic distance (4.361 Å, see structural description), there is very little overlap between the d-orbitals of the copper atoms, so the through-space interaction contribution to the J value is negligible. The magnitude of this weak antiferromagnetic coupling comes from the overlap between the d-orbitals of the metal and the p-orbitals of the bridge ligand [16]

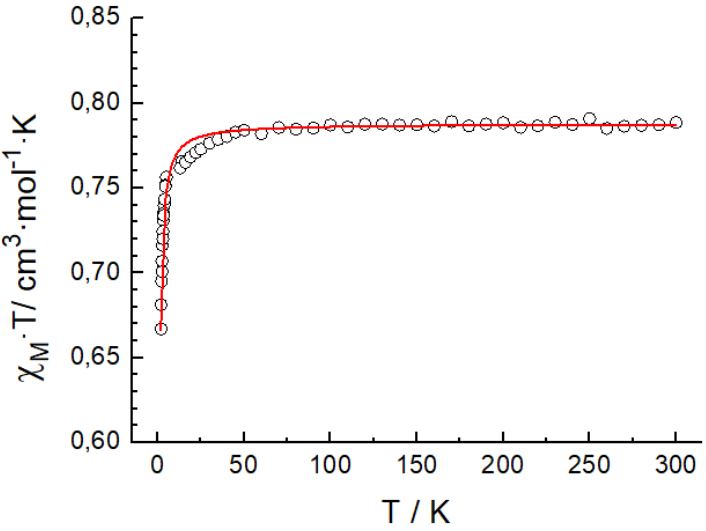


Fig. 13. (a) χMT vs. T plot for compound 1 at 5000 Oe. The solid red line corresponds to the best fit (see text).

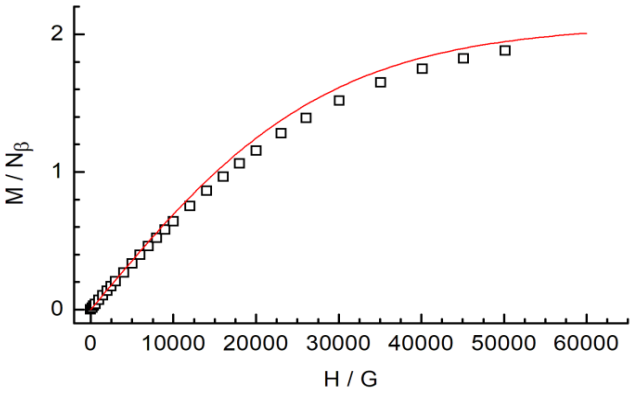


Fig. 14. Plot of the M/Nβ vs. H at 2K for compound 1. The solid red line corresponds to the M/Nβ simulation for two isolated S = 1/2 at 2 K, g = 2.07

## 6.2. MAGNETIC PROPERTIES OF COMPLEX 2

The temperature dependence of $\chi_M T$ ($\chi_M$ being the magnetic susceptibility for two Mn(II) ions) for complex 2 is shown in Figure 15 (from 300 K to 2 K). $\chi_M T$ value is 8.763 $cm^3\ mol^{-1}\ K$ at 300K, a value which is as expected for two "isolated" Mn(II) ions (with g ~ 2.00). Decreasing the temperature, the values of $\chi_M T$ are practically constant to ca. 45 K (8.455 $cm^3 mol^{-1} K$). From this value to 2 K the decrease is more pronounced reaching a value of 5.146 $cm^3 mol^{-1} K$, at 2 K. The shape of this curve is characteristic of the occurrence of weak antiferromagnetic interactions between the Mn(II) centres.

Taking into account the dinuclear nature of complex 2, the susceptibility data were fitted by the equation 2 formula given by Kahn [17] based on the exchange Hamiltonian $H = -JS_iS_j$. The best fit is given by the exchange parameters J = -0.240 ± 0.003 $cm^{-1}$, g = 1.988 ± 0.002 (the standard value for Mn(II) ions) and R = 3.8 x $10^{-5}$, where $R = \Sigma[(\chi_M T)_{exp} - (\chi_M T)_{calc}]^2 / \Sigma[(\chi_M T)_{exp}]^2$.

$$\chi T = \frac{2N_A g^2 \mu^2}{k} \cdot \frac{e^x + 5e^{3x} + 14e^{6x} + 30e^{10x} + 55e^{15}}{1 + 3e^x + 5e^{3x} + 7e^{6x} + 9e^{10x} + 11e^{15}} \qquad \left(x = \frac{-J}{kT}\right) \qquad \text{(Eq. 5)}$$

The magnetization measurements at 2 K up to an external field of 5.5 T confirm the very weak antiferromagnetic interaction. At higher field, the reduced molar magnetization molar M/Nβ units

tends to 9.66 (figure 16). This value is close to the expected for two isolated Mn(II) ion (10 M/Nβ with g = 2.0). Confrontation of the overall shape of the plot of the compound with the Brillouin [2] one (solid plot) for two isolated Mn(II) with S = 5/2 and g = 2.00 at T = 2 K indicates slower saturation which is consistent with the weak antiferromagnetic coupling between the two manganese centres.

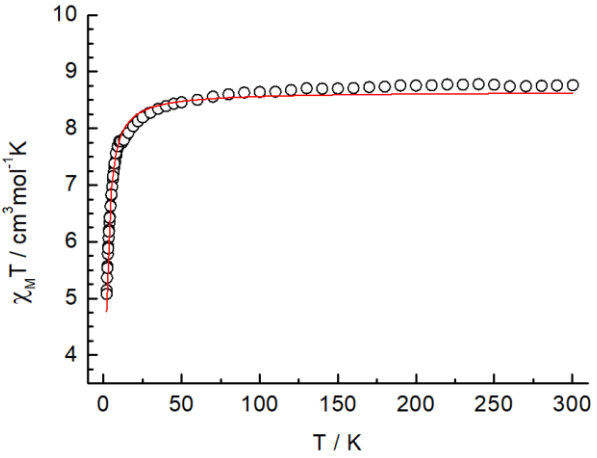


Fig. 15. Plot of $\chi_M T$ vs T for complex 2 The solid red line represents the best-fit calculation (see text).

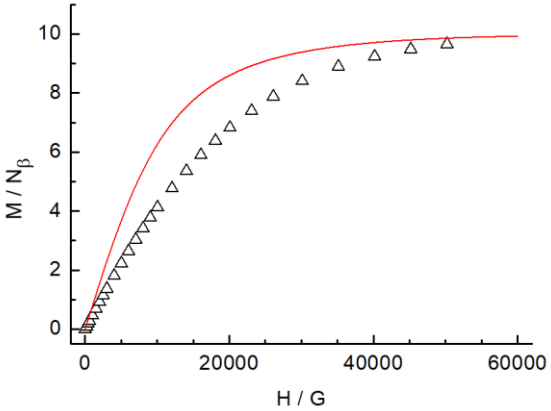


Fig. 16. Plot of the reduced magnetization at 2 K for complex 2, solid line represents the M/Nβ simulation for two isolated S = 5/2 system at 2 K with g = 2.00.

In order to stablish a correlation between the J value and the Mn-Cl-Mn angle, a few examples of already reported manganese complexes containing the $[Mn_2(\mu\text{-}Cl)_2]^{2+}$ unit were found using the CCDC *ConQuest* software[18]. By looking at the values in the table below, it is clear that there is not a clear dependency, although the exchange parameter J seems to increase by increasing the Mn-Cl-Mn angle.

| Mn-Cl-Mn (º) | Mn-Mn (Å) | J (cm-1) | Ref. |
|---|---|---|---|
| 96.59 | 3.859 | 0.15 | [7] |
| 96.42 | 3.850 | 0.55 | [6] |
| 95.84 | 3.777 | -0.17 | [19] |
| 95.72 | 3.835 | 0.68 | [20] |
| 95.52 | 3.726 | 1.49 | [21] |
| 94.53 | 3.850 | -0.24 | This work |
| 93.53 | 3.740 | 0.53 | [22] |
| 92.71 | 3.640 | -0.024 | [23] |
| 90.69 | 3.612 | -5.2 | [24] |

Table 5. Structural parameters and magnetic coupling constant (J) for Mn(II) compounds with a $[Mn_2(\mu\text{-}Cl)_2]^{2+}$ unit.

# 7. EXPERIMENTAL SECTION

## 7.1. MATERIALS AND METHODS

All reagents and solvents were purchased from commercial sources and used without further purification. The Schiff base ligand $H_2L$ was synthetized from the condensation of 2-pyridincarboxaldehyde and 2-amino-1,3-propanol using methanol as a solvent.

## 7.2. PREPARATION OF $H_2L$ LIGAND

A methanolic solution of 10 mmol pyridine-2-carboxaldehyde and 10 mmol of 2-amino-1,3-propanediol in 100 mL of methanol was heated under reflux at 70 ºC for two hours. The solution was allowed to cool down to room temperature and used without further purification. The product was not isolated and left in the freezer for storage.

### 7.3. Syntheses of the complexes

Only the syntheses of the two compounds that were able to crystallize are shown here. In total, 67 syntheses were performed using various metals and ligands. Unfortunately, none of them were able to crystallize.

#### 7.3.1. Synthesis of compound 1

1 mmol of $CuClO_4 \cdot H_2O$ (0.371 g) in methanol (5 mL) was added dropwise to 10 mL (1 mmol) of the L1 ligand solution and stirred for ten minutes. A solution of $DyCl_3 \cdot 6H_2O$ (1mmol, 0.377 g) in methanol (5 mL) was added to the resulting blue solution. The solution turned dark blue after a while and it was allowed to stir overnight. The resulting solution was left in open atmosphere to evaporate. Small crystals not suitable for XRD appeared after four days. They were redissolved in $MeOH/H_2O$ in a 1:1 proportion and left undisturbed in open atmosphere to evaporate. Bigger crystals suitable for XRD were obtained after ten days.

Although we have not experienced any problems, perchlorate salts are explosive and should be handled with care.

#### 9.2.2. Synthesis of compound 2

1 mmol of $MnCl_2 \cdot 4H_2O$ and 1 mmol of $DyCl_3 \cdot 6H2O$, both dissolved in 5 mL of methanol, were added to 10 mL (1 mmol) of the ligand solution and refluxed for 2 h. The formed pale-orange

solution was left undisturbed in open atmosphere. A solid precipitate appeared after two weeks, although it was not in the desired crystalline form. The precipitate was dissolved in methanol (10 mL) and layered with diethyl ether. Medium-sized pale-yellow crystals suitable for XRD appeared after two weeks. Due to lack of material to carry on with the magnetic measurements, the same synthesis was repeated, this time without adding the $DyCl_3 \cdot 6H_2O$, as the lanthanide is not inserted in the structure (see structural description).

# 8. CONCLUSIONS

The Schiff base ligand could not be successfully synthetized. Instead, an interesting new ligand containing an oxazolidine ring has been assembled. Two dinuclear transition metal complexes have been successfully synthetized and their crystal structures have been determined by XRD. In the first compound, two copper (II) complexes of different nuclearity co-crystallize in the same crystal structure. In the second compound, a dinuclear manganese (II) complex bridged by two chloride anions has been successfully characterized. In this case, a second cyclization has taken place in the ligand, leading to a rare double oxazolidine ring coordinated to the metal. Only a few complexes found in literature have a similar ligand coordinated to a transition metal.

Magnetic studies were performed in both compounds. The two metallic centres in both complexes are antiferromagnetically coupled with a very small exchange constant, as expected by looking at their structural properties. These results are in good agreement with those found in literature.

We were not able to insert a lanthanide metal in the complexes. No SMM measurements have been performed in this work.

# 9. REFERENCES AND NOTES


[1] A. Saleem *et al.*, "Transition metal complexes of a versatile polyalkoxy oxazolidine-based ligand derived from: In situ cyclization," *Dalt. Trans.*, vol. 47, no. 17, pp. 6156–6165, 2018, doi: 10.1039/c7dt04634k.

[2] J. Ribas Gispert, *Coordination Chemistry*, 1st ed. Wiley, 2008.

[3] D. A. Atwood, *The rare earth elements. Fundamentals and applications*, 1st ed. Wiley, 2012.

[4] R. Sessoli, D. Gatteschi, and A. Caneschi, "Magnetic bistability in a metal-ion cluster," *Nature*, vol. 365, pp. 141–143, 1993.

[5] B. Lapo and W. Wernsdorfer, "Molecular spintronics using single-molecule magnets," *Nat. Mater.*, vol. 7, pp. 179–186, 2008, doi: 10.1103/PhysRevB.99.245404.

[6] J. Z. Wu, E. Bouwman, A. M. Mills, A. L. Spek, and J. Reedijk, "Manganese(II) complexes of a set of 2-aminomethylpyridine-derived ligands bearing a methoxyalkyl arm: Syntheses, structures and magnetism," *Inorganica Chim. Acta*, vol. 357, no. 9, pp. 2694–2702, 2004, doi: 10.1016/j.ica.2004.02.001.

[7] B. MacHura *et al.*, "Manganese(II) complexes of 2,3,5,6-tetra-(2-pyridyl)pyrazine-Syntheses, crystal structures, spectroscopic, magnetic and catalytic properties," *Polyhedron*, vol. 53, no. 3, pp. 132–143, 2013, doi: 10.1016/j.poly.2013.01.015.

[8] K. Ha, "Crystal structure of di(μ2-chloro)-dichloro-bis(2,3,5,6- tetra-2-pyridylpyrazine)dimanganese(II), Mn2Cl4(C 24H16N6)2," *Zeitschrift fur Krist. - New Cryst. Struct.*, vol. 226, no. 1, pp. 59–60, 2011, doi: 10.1524/ncrs.2011.0029.

[9] J. Mayans, J. Mayans, D. Gómez, M. Font-Bardia, M. Font-Bardia, and A. Escuer, "Chiral Oxazolidine Complexes Derived from Phenolic Schiff Bases," *Cryst. Growth Des.*, vol. 20, no. 6, pp. 4176–4184, 2020, doi: 10.1021/acs.cgd.0c00466.

[10] C. Ding, F. Zeng, J. Ni, B. Wang, and Y. Xie, "Polynuclear complexes of ligands containing in situ formed oxazinane and oxazolidine rings with appended alkoxyl and phenol groups," *Cryst. Growth Des.*, vol. 12, no. 4, pp. 2089–2096, 2012, doi: 10.1021/cg300096n.

[11] S. Karim, A. Chakraborty, D. Samanta, E. Zangrando, T. Ghosh, and D. Das, "A dinuclear iron complex as an efficient electrocatalyst for homogeneous water oxidation reaction," *Catal. Sci. Technol.*, vol. 10, no. 9, pp. 2830–2837, 2020, doi: 10.1039/d0cy00011f.

[12] R. J. Gueue and M. R. Snow, "Crystal Studies of the Reaction Products of Chelate Complexes. I. The Structure of Bis(dihydro- IH,3H,5H-oxazolo[3,4-c]oxazole7a-carboxylato)copper(Il)," *Acta Cryst.*, vol. 33, pp. 510–516, 1977, doi: 10.1107/S0567740877003951.

[13] E. D. Bergmann, "The oxazolidines," *Chem. Rev.*, vol. 53, pp. 309–352, 1953, doi: 10.1021/cr60165a005.

[14] B. Bleaney and K. D. Bowers, "Anomalous paramagnetism of copper acetate," *Proc. R.*

*Soc*, vol. 214, p. 451, 1952.

[15] K. Das *et al.*, "EPR interpretation, magnetism and biological study of a Cu(II) dinuclear complex assisted by a schiff base precursor," *J. Biol. Inorg. Chem.*, vol. 22, no. 4, pp. 481–495, 2017, doi: 10.1007/s00775-016-1428-x.

[16] M. Ehesan Ali and S. N. Datta, "Theoretical investigation of magnetic properties of a dinuclear copper complex [Cu2(μ-OAc)4(MeNHpy)2]," *J. Mol. Struct. THEOCHEM*, vol. 775, no. 1–3, pp. 19–27, 2006, doi: 10.1016/j.theochem.2006.06.043.

[17] "Molecular Magnetism_O-Kahn.pdf." .

[18] "ConQuest 2020." .CCDC

[19] P. Tyagi and U. P. Singh, "Chloro and azido bonded manganese complexes: Synthesis, structural, and magnetic studies," *J. Coord. Chem.*, vol. 62, no. 10, pp. 1613–1622, 2009, doi: 10.1080/00958970802680682.

[20] I. Romero, M. Rodríguez, A. Llobet, M. Corbella, G. Fernández, and M. N. Collomb, "EPR and magnetic properties of [Mn(μ-Cl)2(bpy)]n: An unusual ferromagnetic interaction in a Mn(II) chloro-bridged polymer," *Inorganica Chim. Acta*, vol. 358, no. 15, pp. 4459–4465, 2005, doi: 10.1016/j.ica.2005.08.024.

[21] I. I. Ebralidze, G. Leitus, L. J. W. Shimon, Y. Wang, S. Shaik, and R. Neumann, "Structural variability in manganese(II) complexes of N,N'-bis(2-pyridinylmethylene) ethane (and propane) diamine ligands," *Inorganica Chim. Acta*, vol. 362, no. 13, pp. 4713–4720, 2009, doi: 10.1016/j.ica.2009.06.037.

[22] G. A. Van Albada, A. Mohamadou, W. L. Driessen, R. De Gelder, S. Tanase, and J. Reedijk, "A dinuclear Mn(II) chloro-bridged compound with a weak ferromagnetic Mn-Mn interaction: Synthesis, structure, EPR and magnetism of [Mn(μ-Cl)(2,2'- bi-imidazoline) 2] 2Cl 2," *Polyhedron*, vol. 23, no. 15, pp. 2387–2391, 2004, doi: 10.1016/j.poly.2004.07.019.

[23] W. T. Deng, J. C. Liu, and J. Cao, "Syntheses, crystal structures and properties of four new coordination polymers involving a schiff base ligand bearing an easily abstracted proton in the hydrazone backbone," *Inorg. Chem. Commun.*, vol. 35, pp. 315–317, 2013, doi: 10.1016/j.inoche.2013.07.018.

[24] B. Bräuer *et al.*, "A dimanganese(II) complex with bridging chlorides: Synthesis, electrochemistry, magnetic behavior, structure and bonding," *Inorganica Chim. Acta*, vol. 365, no. 1, pp. 277–281, 2011, doi: 10.1016/j.ica.2010.09.033.

# 10. ACRONYMS

SMM: Single molecular magnet

ZFS: Zero field splitting

XRD: X-Ray diffraction

L1: pyridin-2-yl(2-(pyridin-2-yl)oxazolidin-4-yl)ethoxy)methanolate

L1': 2-(3-(hydroxy(pyridin-2-yl)methyl)-2-(pyridin-2-yl)oxazolidin-4-yl)ethanol

L2: 3,5-di(dipyridin-2-yl)dihydro-1H,3H,5H-oxazolo[3,4-c]oxazole

# APPENDICES

# APPENDIX 1: OTHER STRUCTURES

The crystal structures of unsuccessful syntheses are reported here.

## $[CuCl(py)_4]^+$

As we can see in this structure, the strong coordinating ability of the pyridine drives the formation of the complex and avoids the coordination of the metal with the desired ligand. The same structure is already reported in the literature and lacks interesting magnetic properties, so no further measurements have been performed.

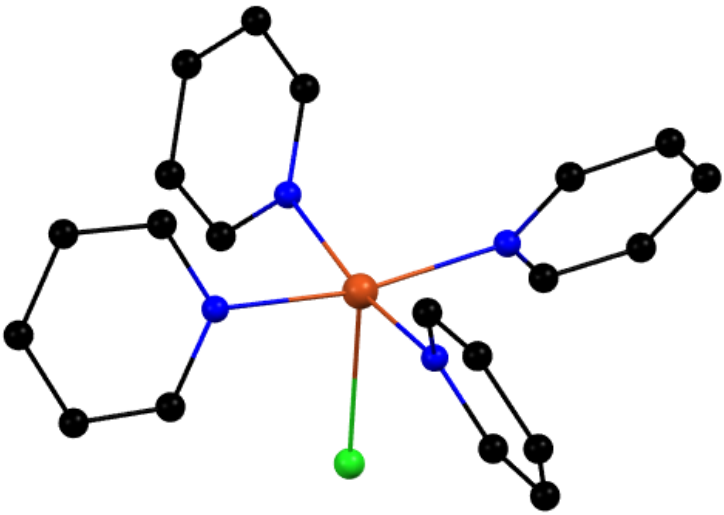

Fig. 17. Crystal structure obtained (Colour code: orange, copper; green, chlorine; blue, nitrogen; black, carbon)

# APPENDIX 2: CRYSTALLOGRAPHIC DATA

**Crystal Structure Report for I55ZB55 (compound 1)**

A blue prism-like specimen of C60H70Cl6Cu4N12O31, approximate dimensions 0.160 mm x 0.190 mm x 0.200 mm, was used for the X-ray crystallographic analysis. The X-ray intensity data were measured on a D8 Venture system equipped with a multilayer monochromator and a Mo microfocus (λ = 0.71073 Å).

The frames were integrated with the Bruker SAINT software package using a narrow-frame algorithm. The integration of the data using a triclinic unit cell yielded a total of 74097 reflections to a maximum θ angle of 30.55° (0.70 Å resolution), of which 10945 were independent (average redundancy 6.770, completeness = 99.0%, Rint = 2.72%, Rsig = 1.66%) and 10125 (92.51%) were greater than 2σ(F2). The final cell constants of a = 10.6886(7) Å, b = 11.9370(8) Å, c = 16.1341(10) Å, α = 108.127(2)°, β = 97.404(2)°, γ = 107.698(2)°, volume = 1806.1(2) Å3, are based upon the refinement of the XYZ-centroids of reflections above 20 σ(I). Data were corrected for absorption effects using the Multi-Scan method (SADABS). The calculated minimum and maximum transmission coefficients (based on crystal size) are 0.6920 and 0.7461.

The structure was solved and refined using the Bruker SHELXTL Software Package, using the space group P -1, with Z = 1 for the formula unit, $C_{60}H_{72}Cl_6Cu_4N_{12}O_{31}$. The final anisotropic full-matrix least-squares refinement on $F^2$ with 535 variables converged at R1 = 2.66%, for the observed data and wR2 = 7.10% for all data. The goodness-of-fit was 1.044. The largest peak in the final difference electron density synthesis was 0.857 $e^-/Å^3$ and the largest hole was -0.665 $e^-/Å^3$ with an RMS deviation of 0.064 e-/Å3. On the basis of the final model, the calculated density was 1.769 g/cm3 and F(000), 982 e-.

Crystallographic author: Mercè Font-Bardia, Unitat de Difracció de RX. Centres Científics i Tecnològics de la Universitat de Barcelona (CCiTUB). Universitat de Barcelona. Solé i Sabarís 1-3. 08028-Barcelona

| | |
|---|---|
| Identification code | I55ZB55_0m_a |
| Empirical formula | $C_{60}$ $H_{72}$ $Cl_6$ Cu4 Dy0 $N_{12}$ $O_{31}$ |
| Formula weight | 1924.15 |
| Temperature | 100(2) K |
| Wavelength | 0.71073 Å |
| Crystal system | Triclinic |
| Space group | P -1 |
| Unit cell dimensions | a = 10.6886(7) Å α= 108.127(2)°. |
| | b = 11.9370(8) Å β= 97.404(2)°. |
| | c = 16.1341(10) Å γ= 107.698(2)°. |
| Volume | 1806.1(2) Å3 |
| Z | 1 |
| Density (calculated) | 1.769 Kg/$m^3$ |
| Absorption coefficient | 1.482 $mm^{-1}$ |
| F(000) | 982 |
| Crystal size | 0.200 x 0.190 x 0.160 $mm^3$ |
| Theta range for data collection | 2.527 to 30.547°. |
| Index ranges | -15<=h<=15, -17<=k<=17, -23<=l<=23 |
| Reflections collected | 74097 |
| Independent reflections | 10945 [R(int) = 0.0272] |
| Completeness to theta = 25.242° | 99.2 % |
| Absorption correction | Semi-empirical from equivalents |
| Max. and min. transmission | 0.7461 and 0.6920 |
| Refinement method | Full-matrix least-squares on F2 |

| | |
|---|---|
| Data / restraints / parameters | 10945 / 6 / 535 |
| Goodness-of-fit on F2 | 1.044 |
| Final R indices [I>2sigma(I)] | R1 = 0.0266, wR2 = 0.0678 |
| R indices (all data) | R1 = 0.0300, wR2 = 0.0710 |
| Extinction coefficient | n/a |
| Largest diff. peak and hole | 0.857 and -0.665 e/Å$^3$ |

Table 6. Crystal data and structure refinement for I55ZB55_0m_a.

**Crystal Structure Report for I55ZB74A (compound 2)**

A colorless prism-like specimen of $C_{63}H_{72}Cl_8Mn_4N_{12}O_{11}$, approximate dimensions 0.100 mm x 0.120 mm x 0.150 mm, was used for the X-ray crystallographic analysis. The X-ray intensity data were measured on a D8 Venture system equipped with a multilayer monochromator and a Mo microfocus (λ = 0.71073 Å).

The frames were integrated with the Bruker SAINT software package using a narrow-frame algorithm. The integration of the data using a monoclinic unit cell yielded a total of 30283 reflections to a maximum θ angle of 30.53° (0.70 Å resolution), of which 5462 were independent (average redundancy 5.544, completeness = 98.6%, Rint = 2.65%, Rsig = 2.07%) and 4848 (88.76%) were greater than 2σ(F2). The final cell constants of a = 20.5981(8) Å, b = 11.0699(4) Å, c = 17.4397(7) Å, β = 114.596(2)°, volume = 3615.8(2) Å3, are based upon the refinement of the XYZ-centroids of reflections above 20 σ(I). Data were corrected for absorption effects using the Multi-Scan method (SADABS). The calculated minimum and maximum transmission coefficients (based on crystal size) are 0.6615 and 0.7461.

The structure was solved and refined using the Bruker SHELXTL Software Package, using the space group C 1 2/c 1, with Z = 2 for the formula unit, $C_{63}H_{72}Cl_8Mn_4N_{12}O_{11}$. The final anisotropic full-matrix least-squares refinement on F2 with 229 variables converged at R1 = 3.96%, for the observed data and wR2 = 10.84% for all data. The goodness-of-fit was 1.068. The largest peak in the final difference electron density synthesis was 1.136 e$^-$/Å$^3$ and the largest hole was -0.839 e-/Å3 with an RMS deviation of 0.090 e$^-$/Å$^3$. On the basis of the final model, the calculated density was 1.540 g/cm$^3$ and F(000), 1716 e$^-$.

Crystallographic author: Mercè Font-Bardia, Unitat de Difracció de RX. Centres Científics i Tecnològics de la Universitat de Barcelona (CCiTUB). Universitat de Barcelona. Solé i Sabarís 1-3. 08028-Barcelona

| | |
|---|---|
| Identification code | I55ZB74A_0m_a |
| Empirical formula | $C_{63}$ $H_{72}$ $Cl_8$ $Mn_4$ $N_{12}$ $O_{11}$ |
| Formula weight | 1676.68 |
| Temperature | 100(2) K |
| Wavelength | 0.71073 Å |
| Crystal system | Monoclinic |
| Space group | C 2/c |
| Unit cell dimensions | a = 20.5981(8) Å α= 90° |
| | b = 11.0699(4) Å β= 114.596(2)° |
| | c = 17.4397(7) Å γ = 90° |
| Volume | 3615.8(2) $Å^3$ |
| Z | 2 |
| Density (calculated) | 1.540 $Kg/m^3$ |
| Absorption coefficient | 1.044 $mm^{-1}$ |
| F(000) | 1716 |
| Crystal size | 0.150 x 0.120 x 0.100 mm3 |
| Theta range for data collection | 2.248 to 30.528°. |
| Index ranges | -29<=h<=29, -15<=k<=15, -22<=l<=24 |
| Reflections collected | 30283 |
| Independent reflections | 5462 [R(int) = 0.0265] |
| Completeness to theta = 25.242° | 99.2 % |
| Absorption correction | Semi-empirical from equivalents |
| Max. and min. transmission | 0.7461 and 0.6615 |
| Refinement method | Full-matrix least-squares on F2 |

| | |
|---|---|
| Data / restraints / parameters | 5462 / 2 / 229 |
| Goodness-of-fit on F2 | 1.068 |
| Final R indices [I>2sigma(I)] | R1 = 0.0396, wR2 = 0.1024 |
| R indices (all data) | R1 = 0.0471, wR2 = 0.1084 |
| Extinction coefficient | n/a |
| Largest diff. peak and hole | 1.136 and -0.839 $e^{-}$/Å$^3$ |

Table 7. Crystal data and structure refinement for I55ZB74A_0m_a.